Shahrood University of Technology
Iranian Society of Mining Engineering (IRSME)
Journal of Mining and Environment (JME)
journal homepage: www.jme.shahroodut.ac.ir
THOMSON REUTERS

Vol. 10, No. 4, 2019, 1061-1081.
DOI: 10.22044/jme.2019.8687.1752

Geostatistical and multi-fractal modeling of geological and geophysical characteristics in Ghalandar Skarn-Porphyry Cu Deposit, Iran

S. Salarian[1], O. Asghari[1*], M. Abedi[2] and S.K. Alilou[3]

1. Simulation and Data Processing Lab, School of Mining Engineering, College of Engineering, University of Tehran, Tehran, Iran
2. Geoexploration Targeting Lab, School of Mining Engineering, College of Engineering, University of Tehran, Tehran, Iran
3. School of Mining Engineering, College of Engineering, University of Tehran, Tehran, Iran

Received 12 July 2019; received in revised form 8 August 2019; accepted 8 August 2019

Keywords

Multi-Fractal Model
Geostatistics
Electrical Chargeability
Electrical Resistivity
Magnetic Susceptibility

Abstract

This work aims at figuring out the spatial relationships between the geophysical and geological models in a case study pertaining to copper-sulfide mineralization through an integrated 3D analysis of favorable target. The Ghalandar Skarn-Porphyry Cu Deposit, which is located in NW Iran, is selected for this research work. Three geophysical surveys of direct current electrical resistivity and induced polarization tomography along with magnetometry are performed to construct the physical properties of electrical resistivity, chargeability, and magnetic susceptibility, respectively. Inverse modeling and geostatistical interpolation are utilized to generate the physical 3D models. A 3D model of Cu grade is generated using ordinary kriging; however, the indicator kriging method is run to design a 3D model of rock types through incorporating the drilling results. Block models of geophysical and geological characteristics are cast in a similar 3D mesh to investigate their relationships in copper mineralization. A concentration-volume multi-fractal method is utilized to divide each model into its sub-sets, where the most productive portions in association with Cu-bearing mineralization are distinguished. Note that sub-sets of geophysical models are spatially matched with geological models of Cu grade and rock types. The zones with low electrical resistivity, high chargeability, and low magnetic susceptibility correspond to the main source of Cu mineralization in a dominated skarn rock type setting.

1. Introduction

Integration of soft and hard data is utilized to create a realistic geological model by incorporating different sources of information. The exploratory geospatial hard data (e.g. borehole data) is the direct measurement of what is being modeled, while the soft data is everything else (e.g. geophysical measurements) [1]. Geological models reflecting the geometry of mineral targets are required to be consistent with different types of information. Taking several types of geospatial dataset collected over the studied area into account can reduce the ambiguity arising from sophisticated favorable targets, and enhance the reliability of the results [2]. The borehole data usually cannot provide enough data because of low spatial density in relation to the complexity of the sub-surface to be mapped but geophysical measurements can be surveyed affordably in a dense data coverage as they construct a 3D representation of physical property model through inverse modeling [3].

Direct current electrical surveys are useful for exploration of both the metallic and non-metallic mineral resources [4]. The induced polarization (IP) and resistivity (Rs) methods have become more applicable and popular after improvements made in the past two decades with modern measurement tools and computer applications [5]. The variability of appropriate mineral deposits can make interpretations of electrical data more

Corresponding author: o.asghari@ut.ac.ir (O. Asghari).

challenging [6]. The IP method has been utilized as the main tool to explore the high concentration sulfide deposits (e.g. porphyry and skarn copper deposits). Experiments have proved that most of the sulfide content targets indicate larger polarization effects in comparison with silicates and iron oxides [7]. Nevertheless, IP responses are influenced by both the concentration of minerals and complex physical conditions arising from background geological setting. The behavior of the electric current has also been controlled by these conditions [8, 9]. Note that the electrical resistivity of skarn targets tends to be high but the chargeability response of these rocks highly depends on the presence of sulfide contents [10].

The porphyry copper deposits are generally related to stocks of felsic and porphyritic nature, while these intrusive systems are mostly emplaced in volcanic systems over down going plates in island arc or Andean settings [11]. They provide a high geophysical magnetic response. The propylitic and phyllitic alterations in association with skarn-porphyry Cu deposits destruct magnetite in these volcanics, which may subsequently cause a low magnetic response over magmatic intrusions. Note that a felsic porphyry target is usually ferromagnetic, and sometimes a sharp localized magnetic high may happen in the center of such magnetic low. This system generates a sign of porphyry copper deposit that is indirectly related to the mineralization. Skarn deposits are also generated by replacement of carbonates during metasomatism. These kinds of rocks are generally found near the contact of igneous plutons and sedimentary rocks [12], which have different magnetic susceptibilities (sometimes even remnant magnetizations) compared to the host environment [10]. Therefore, magnetic anomaly can work as a footprint of skarn-porphyry Cu deposits.

The geological and geophysical models of skarn-porphyry type deposits can be divided into some subsets in terms of alteration, rock types, and physical properties, where each subset of physical models can be controlled by geological characteristics. In order to divide each model into its subsets, a concentration-volume (C-V) multi-fractal model can be an appropriate tool in 3D studies. Fractal can explain the complexity in the distribution of data by estimation of data fractal dimensions. Differences in fractal dimensions can describe many spatial processes. The fractal theory was established and developed by Mandelbrot (1983), and was later widely used in various branches of earth sciences. The fractal analysis methods can be utilized by researchers along spatial resolution obtained from geospatial dataset analysis to find the relationships between mineralogical, geochemical, geological, and geophysical signatures [13, 14]. The use of fractal models has led to a better understanding of geophysical phenomena from the micro to the macro level [15, 16]. This method is utilized for different subsets of geophysics such as separating anomaly from background, signal analysis, and geomagnetic polarity analysis [17, 18]. Fractal methods can help to investigate the relationships between the geophysical features and the spatial information of analysis of mineral deposit occurrence data [19, 20]. Fractal dimensions correspond to variations in physical attributes [16, 21]. Thus fractal dimensions of geophysical data variations bring helpful and applicable information about identifying mineralization areas [19].

The purpose of this work was to distinguish the geophysical anomalies from the background data, utilizing a C-V multifractal method, where the physical property models are divided into some subsets to find their relationship with geological characteristics. The aforementioned model was suggested by Afzal *et al*. (2011), and was considered as an appropriate way to explain the spatial distribution of different attributes within the different ore bodies [22, 23]. Significance of the concentration component in the C-V fractal analysis makes the estimation accuracy of concentration a crucial issue. Thus choosing a proper estimation method is required to correctly run a C-V multi-fractal analysis [21].

Integration of geophysical modeling in geostatistical interpolation has been utilized to tackle problems of geological modeling. Abedi *et al*. (2014) have incorporated magnetic data as a secondary soft variable in the grade modeling of a deposit. They applied the multivariate kriging method to interpolate an undersampled grid of iron grade from borehole drilling. Since the iron grade and magnetic susceptibility have a remarkable correlation, this physical property has been utilized as a dense soft variable in grade estimation through geostatistical modeling [24]. In addition, Asghari *et al*. (2016) examined multivariate geostatistics based on geo-electrical properties for estimation of copper grade to decrease the estimation variance and uncertainty. This method can be beneficial when a sporadic pattern of drilling exists. In this case, the sulfide factor (as a ratio of electrical chargeability to electrical resistivity) was utilized as a secondary

correlated variable to estimate the distribution of Cu grade. The results obtained verified that incorporating soft variable yields good results in comparison with ordinary kriging when running a single variable estimation [25].

This work focuses on the Ghalandar deposit as a Cu-sulfide mineralization that is located in the East Azerbaijan Province in Iran. The main motive of the work was to localize and extract anomalous copper zones through electrical and magnetometry surveys. Physical models of electrical resistivity, chargeability, and magnetic susceptibility were constructed in 3D through inverse modeling and geostatistical interpolation. These models were classified into some subsets (zones) through the C-V multi-fractal approach to search for their relationships with the geological characteristics. The 3D models of Cu grade along with rock type were prepared by ordinary and indicator kriging, respectively. They presented that anomalous physical models were in close association with the main zones of mineralization.

The remainder of this work has been prepared as what follows. The second section concisely presents the formulation of ordinary and indicator kriging, and then explains the C-V multi-fractal approach. The geological setting of the Ghalandar skarn-porphyry Cu deposit is explained in the third section. In the fourth section, the geophysical and geological models are constructed, where inverse modeling and geostatistical interpolation are utilized. The C-V multi-fractal is employed in the discussion section to find the spatial relationships between the physical models and Cu-bearing zones. Finally, all achievements are summarized in the conclusion section.

2. Methodology

The following sub-sections describe the formulation of the kriging and C-V multi-fractal methods, respectively.

2.1. Ordinary and indicator kriging methodology

The highly noted kriging method, which is known as the best unbiased linear estimator, was utilized in this work. In addition to constraining the formulation for generating the lowest estimation variance, this method can guarantee the estimations to be unbiased, provided that the selected regional variable is normally distributed [26]. The outcome of the kriging method is minimization of an anticipated variance error based on weight calculation. There are a variety of kriging methods that have differences in how they treat the local or stationary domain mean that is shown as conditions on the set of weights. The ordinary kriging (OK) method works on the basis of the minimum variance linear estimate at locations where the actual values are unknown [27].

The indicator kriging (IK) estimation is a non-parametric approach, meaning that this method does not make the estimated distribution a priori. The IK method can manage extremely variable natural phenomena without any capping extraordinary values or non-linear transformation [28]. This method aims at modeling complex mineralization with non-Gaussian structure. Indeed, these structures include asymmetric spatial continuity of high and low values. The indicator approach categorizes the data into 1 and 0 depending on the relationship with a cut-off value for a given value.

$$i\left(x;z_k\right)=\begin{cases}1 & if \quad z\left(x\right)\geq z_k\\ 0 & if \quad z\left(x\right)<z_k\end{cases} \tag{1}$$

In this formalism, z_x is a given continuous value with a threshold/cut-off of z_k. This is a non-linear transformation of the data value into the binary code of 1 or 0. The kriging indicator-transformed data provides a product value between 0 and 1 for each estimated point. This is an estimate of the ratio of the values in the neighborhood that are greater than the cut-off value. The outcome of IK is a data distribution near the point to be estimated. This distribution is termed a conditional cumulative distribution function. The mentioned distribution of values has been used for many goals, in addition to simply deriving the expected value. Relevant criteria can be utilized to derive the estimate required, not simply the average of the local distribution [29].

Indicator variogram can provide information about the spatial distribution of each class of values, allowing the evaluation of the probability to exceed cut-off values. This variogram value measures how often two distinct points belong to different categories, above or below a pre-defined cut-off [30].

The main incentive of using IK in geoscience applications arises from its non-parametric characteristic. Furthermore, the mixed data populations can be dealt with using the IK algorithms. As IK divides the overall sample distribution with several thresholds, it is not necessary to fit or take a specific

analytically-derived distribution model for the data [29]. Note that another merit of this method is that there is no need for a back-transform. IK can be applied equally to both categorical and continuous variables. The indicator approach lends itself to the estimation of variables that have discrete values such as rock type or lithology. In the mentioned cases, categorical IK will generate the probability of a given rock type code occurring at a certain location. Therefore, probability maps of given lithologies or rock types based on rock code data can be produced [29].

2.2. C-V multi-fractal methodology

The fractal concentration-area method was suggested by Cheng *et al*. (1994) in order to separate the anomalous regions from the background to characterize the distribution of major, minor, and trace element concentrations of ore deposit. The general form of this model can simply be described as follows:

$$A(\rho \le v) \propto \rho^{-\alpha 1}; A(\rho \ge v) \propto \rho^{-\alpha 2} \quad (2)$$

In this equation, $A(\rho \le v)$ and $A(\rho \ge v)$ are areas with elemental concentration values (ρ) that are less than and greater than the contour value ρ, v indicates the threshold values that outline the boundaries between different zones, and $\alpha 1$ and $\alpha 2$ are the characteristic exponents. Certain concentration contours indicating break-points in the log-log plots of concentration contours against areas are considered threshold values distinguishing geochemical or geophysical populations [31]. It has been proposed that the C-A method is valid for volumetric extensions because distributions of elements in a certain direction are in accordance with the fractal models [31, 32]. Consequently, the C-V fractal model can be expressed in the following general form:

$$V(\rho \le v) \propto \rho^{-\alpha 1}; V(\rho \ge v) \propto \rho^{-\alpha 2} \quad (3)$$

In this equation, $V(\rho \le v)$ and $V(\rho \ge v)$ are two volumes with elemental concentration values (ρ) that are less than and greater than the contour value ρ, v indicates the threshold values that outline boundaries between different zones, and $\alpha 1$ and $\alpha 2$ are the characteristic exponents. This equation can be converted to a simple form, as follows:

$$V(\rho) \propto \rho^{-\alpha} \quad (4)$$

where $V(\rho)$ denotes the volume with concentration values lower than ρ defining that zone. In the log-log plot of the C-V curve, certain concentration contours showing break-points in the plots are considered the threshold values to segregate variable populations [21].

3. Geological setting of Ghalandar Skarn-Porphyry Cu deposit

The north dipping subduction of the Neo-Tethys Ocean starting at the Mesozoic formed the Iranian plateau [33, 34]. Upon maturing the subduction zone and the overlying continental magmatic arc, igneous activities led to a thick belt of mostly Cenozoic volcanic/plutonic units that are named in Iran as the Urumieh-Dokhtar magmatic assemblage zone (UDMA), depicted in Figure 1, whereby a distinct and linear intrusive-extrusive complex located between and parallel to the Sanandaj-Sirjan metamorphic zone (SSZ) and the central Iran domain occurred [35]. The Agh-Daragh prospect zone, as the region of interest in this work, is located at the UDMA zone. UDMA is indeed the main host of porphyry-type and epithermal metallic mineralization systems by generating the enormous economically valuable deposits of Cu, Au, and Mo in Iran [36, 37]. This zone has thickened in a range of about 50-100 km, which mostly consists of an Andean-type magmatic arc in adjacency to the Central Iranian Micro-Continent (CIMC). UDMA is characterized in the structural geology map of Iran by Cenozoic extrusive and intrusive rocks of Eocene-Quaternary age and associated volcanoclastic rocks. Note that magmatic intrusions are mostly dominated by the sub-volcanic porphyritic granitoid units of granite, granodiorite, diorite, and tonalite [38, 39].

The simplified geological setting of the Agh-Daragh is presented in Figure 2a. In the western portions of the area and the north of the granodiorite masses, there are a series of green tuffs and volcanic ashes in terms of time associated with Cretaceous era. In the NE of the Gavdel village, there is a sedimentary unit. The color of this unit is dark gray, and it is generally composed of shale and limestone units. The main plutonic mass in the region, closely related to the plutonic mass of the Shiverdagh, is a porphyry granodiorite unit, which includes pink feldspar (sometimes with grains bigger than 1 cm). In some portions, the surface of the intrusive masses has been severely weathered. In terms of mineralogy constituents, they comprise

plagioclase, alkali feldspar, quartz, and hornblende. Quaternary sediments in the shape of conglomerate have covered the region, mostly forming agricultural lands [41].

Ghalandar deposit that encompasses the Ayran Goli and Gowdal mineralization is located about 23 km away from the north of Ahar City, East Azerbaijan Province, NW Iran. This area consists of Eocene and Oligocene lithological layers created by intrusion of massive volcanic rocks into a carbonated host, leading to the formation of Cu-Fe skarn-type mineralization (Figures 2a and 2b). Previous studies have reported that favorability for Cu-Fe mineralization is evident in this region, where the main genetic models of Ghalandar deposit are in the forms of porphyry and skarn. The porphyry system has dominated the SE portions, while the skarn system locates at the western regions [42, 43]. Figure 2a shows the regional geological map of the Agh-Daragh prospect zone, whilst the detailed geological setting of the Ghalandar Cu-Fe porphyry-skarn deposit is portrayed in Figure 2b. The layout of electrical resistivity tomography and magnetic surveys is superimposed on Figure 2b. In addition, after modeling geophysical data, sixteen boreholes were drilled to create the geometry of Cu mineralization for investigating its mining potential.

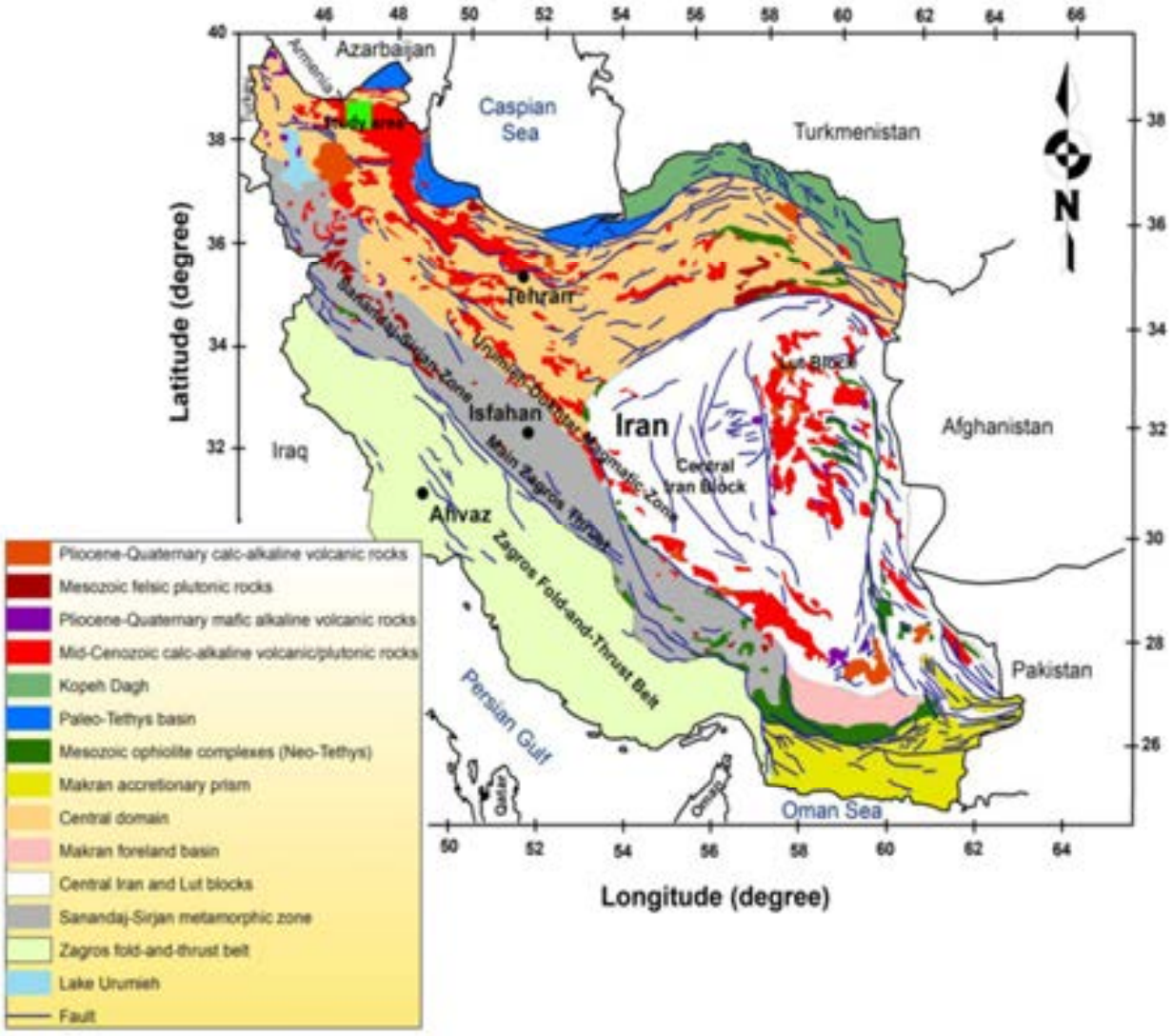

Figure 1. Geological map of Iran and location of the studied area (reproduced with permission of Richards et al. 2006) [40].

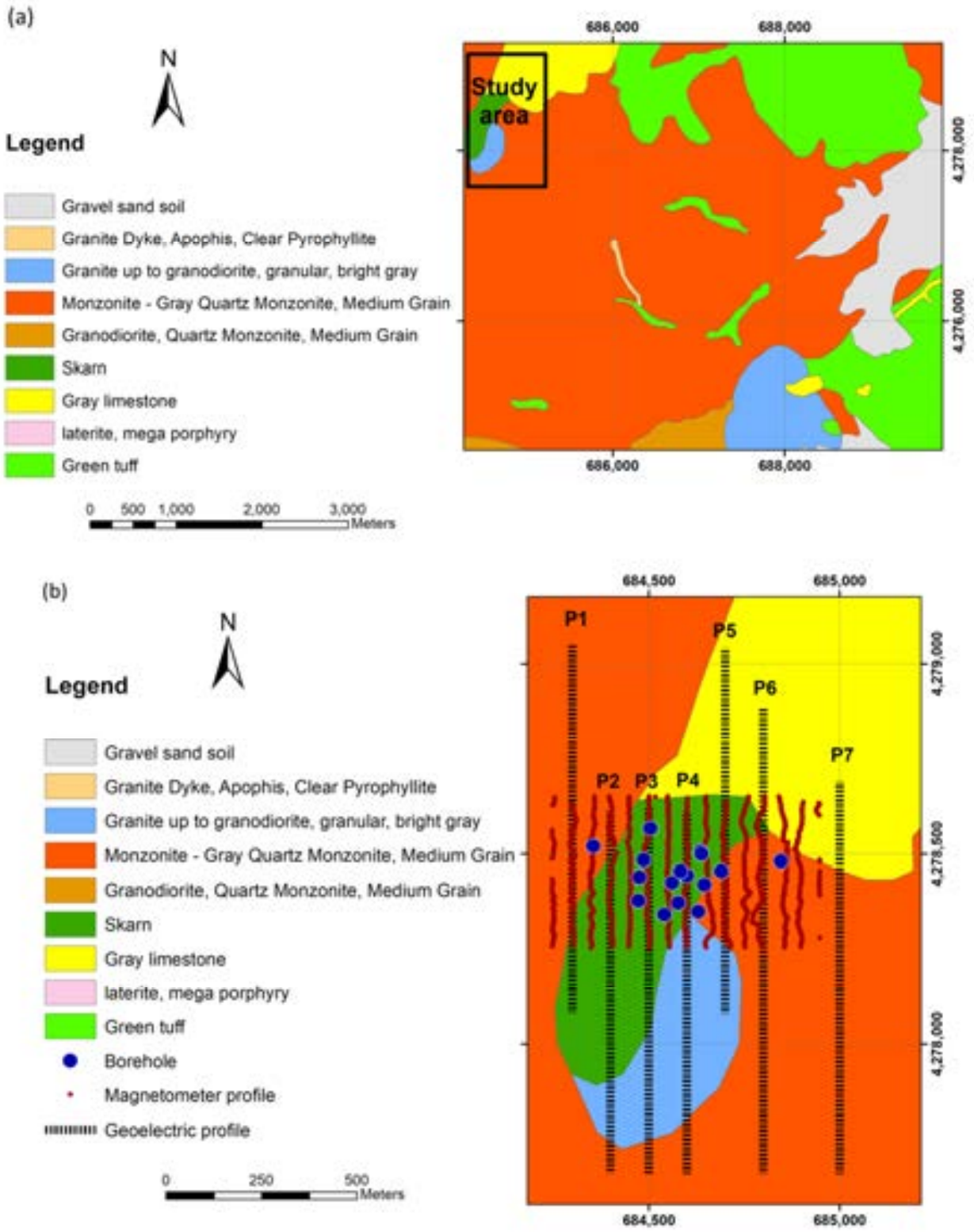

Figure 2. 1:25,000 scale geology map of the Agh-Daragh prospect zone (a), detailed geological setting of the Ghalandar Cu-Fe porphyry-skarn deposit (b).

4. 3D modeling of Ghalandar deposit

The following sub-sections describe the procedure of 3D geological and geophysical modeling of Cu deposit through geostatistical data interpolation and geophysical data inversion, respectively.

4.1 Geological models

In this section, the procedure of building 3D models of Cu grade and rock type from boreholes is discussed. All the sixteen boreholes were drilled vertically in this work. The boreholes

cover a total length of about 2760 m. 3D visualization of all drilling superimposed by the surface topography is indicated in Figure 3. The statistical descriptions of Cu grade derived from boreholes are summarized in Table 1. The histogram and box-plot of this variable were illustrated in Figure 4 (4th row). Before generating those 3D geological models, it is required to produce a block model. Assuming a fixed length and width of 20 m and a height of 10 m for each voxel, the 3D blocky model was generated to surround all drilling. These dimensions were chosen according to the average distance between the boreholes. Since a 3D covariance model is necessary for running geostatistical-based interpolation methods, the directional variogram model is required to be plotted. The directional variogram models for the Cu grade and rock-type variables were searched, and subsequently, the variogram models with the highest spatial continuity were selected based on a trial-and-error test in several directions.

The fitted variogram models are shown in Figure 5. Table 2 lists the parameters of each variogram model. After finding the required inputs for implementing the kriging, 3D models of Cu sulfide grade and rock type were created (Figures 6a and 6b). The point that should be noted is that the 3D model of Cu grade was created using OK but the IK method was performed to design a 3D model of rock type. There were several rock types in the studied area that were grouped into two main types, namely porphyry and skarn. Based on the borehole analysis, 85% of the rocks have been dominated by the skarn type. In the geostatistical data analysis, the variance (sill of variogram) of the indicator data is equal to the multiplication of the percentage of the indicators. It can be seen in Figure 5a that the sill of indicator variogram has reached approximately to this proportion (0.85×0.15).

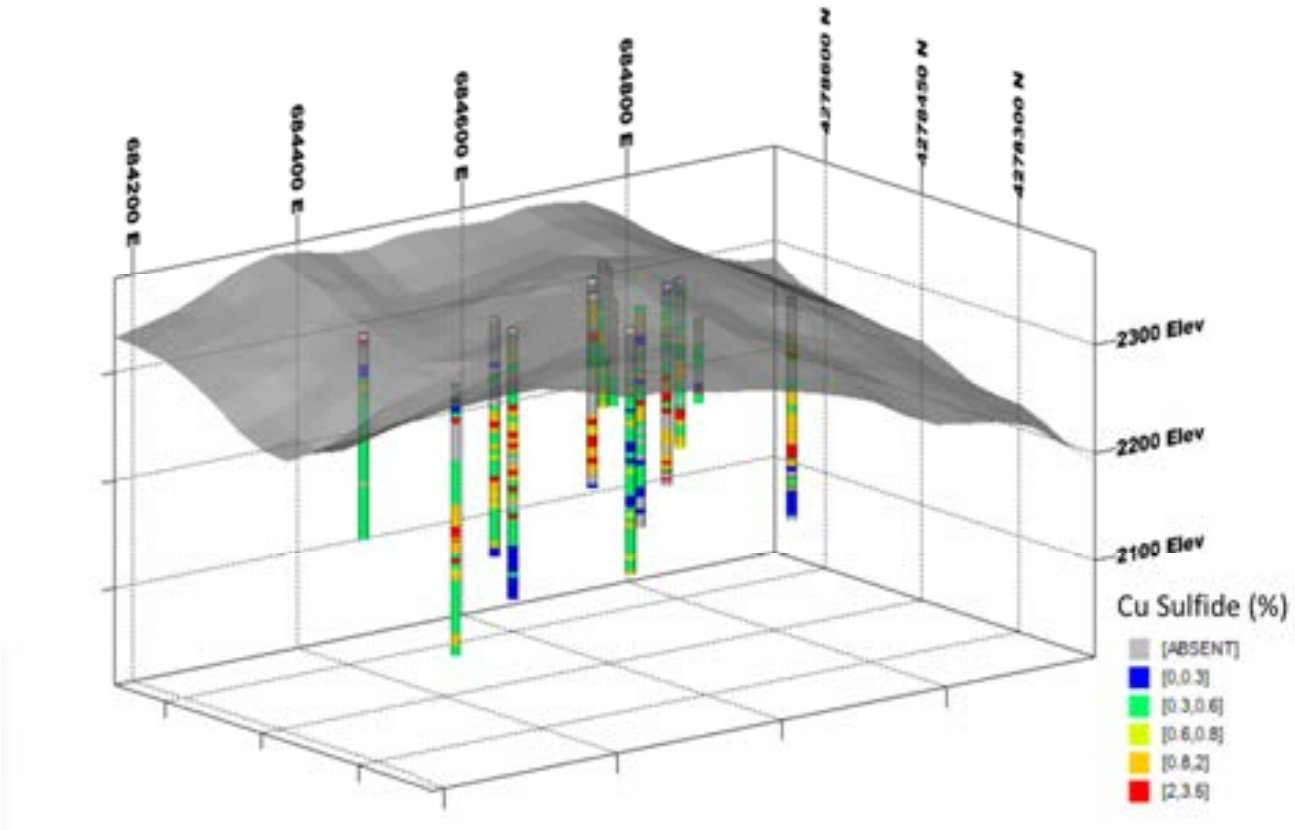

Figure 3. Location map of boreholes with topography surface in the studied region.

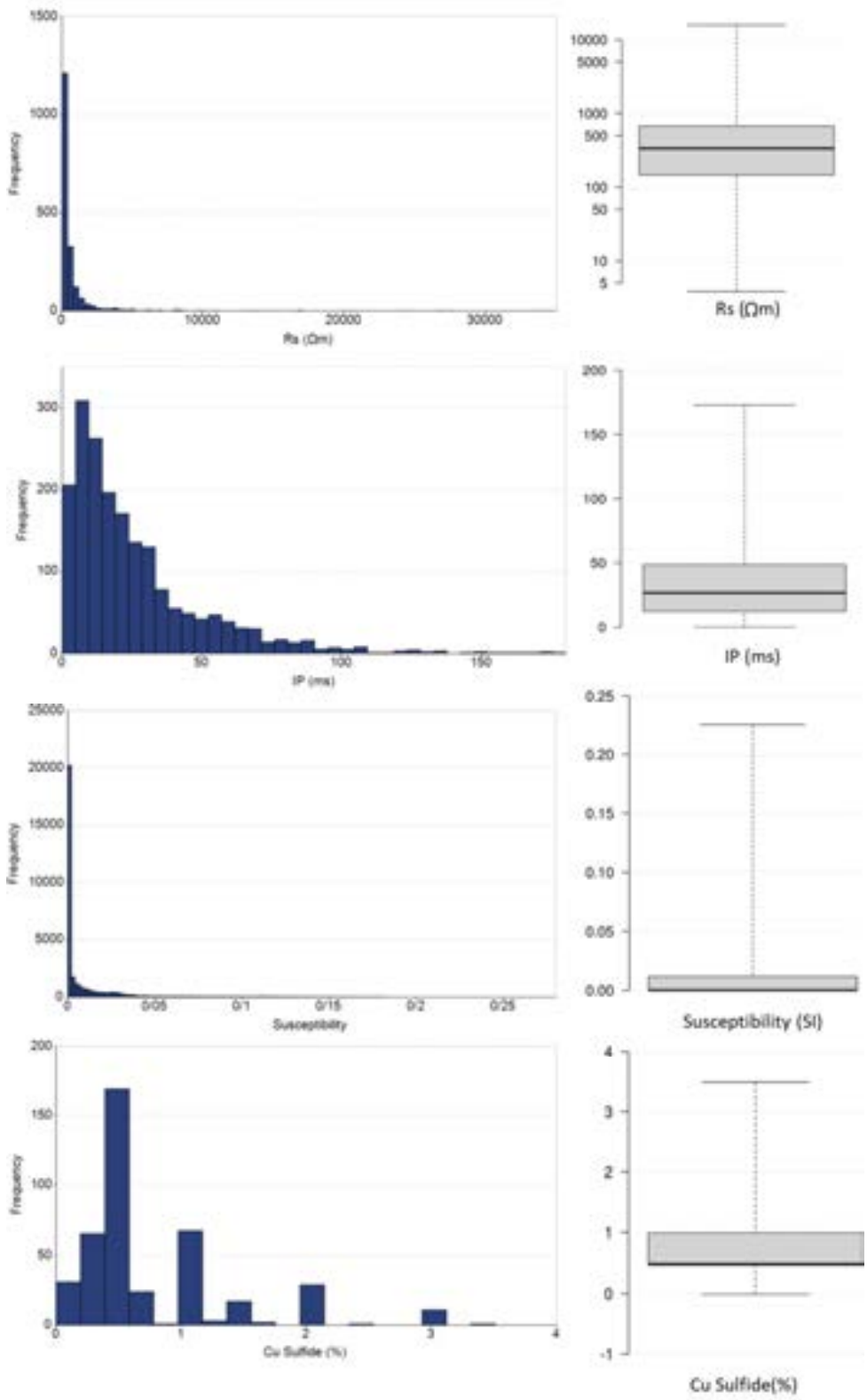

Figure 4. Statistical charts of histogram plot and box-plot for the electrical resistivity (1st row), chargeability (2nd row), magnetic susceptibility (3rd row), and Cu concentration (4th row).

Table 1. Statistical summary of the drilled boreholes.

	Number	Mean	Variance	Maximum	Upper quartile	Median	Lower quartile	Minimum
Cu Sulfide (%)	378	0.75	0.39	3.5	1	0.5	0.5	0

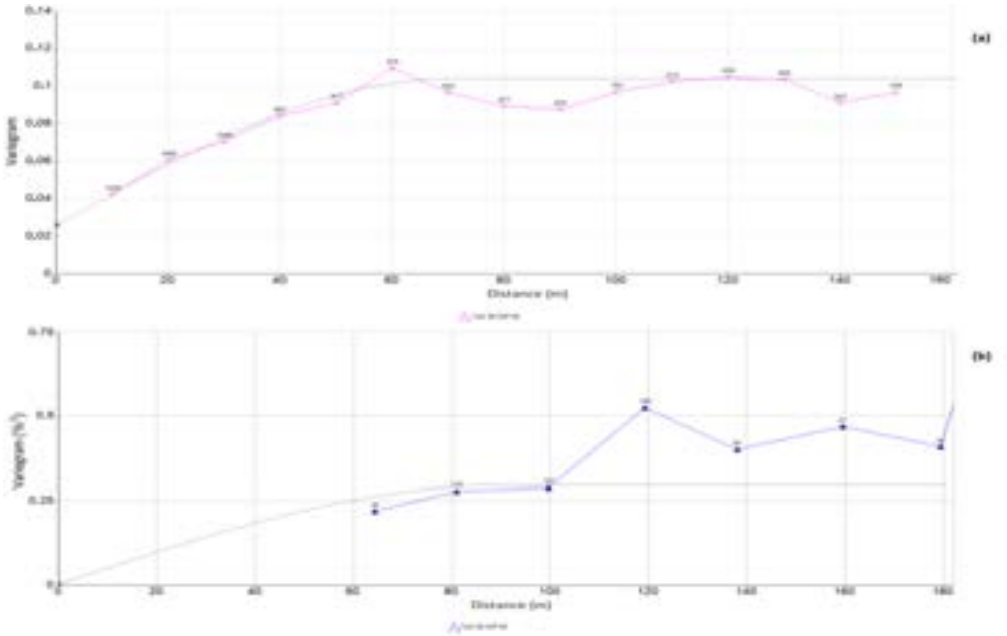

Figure 5. Experimental directional semi-variogram, models, and number of pairs for the (a) rock type and (b) Cu grade.

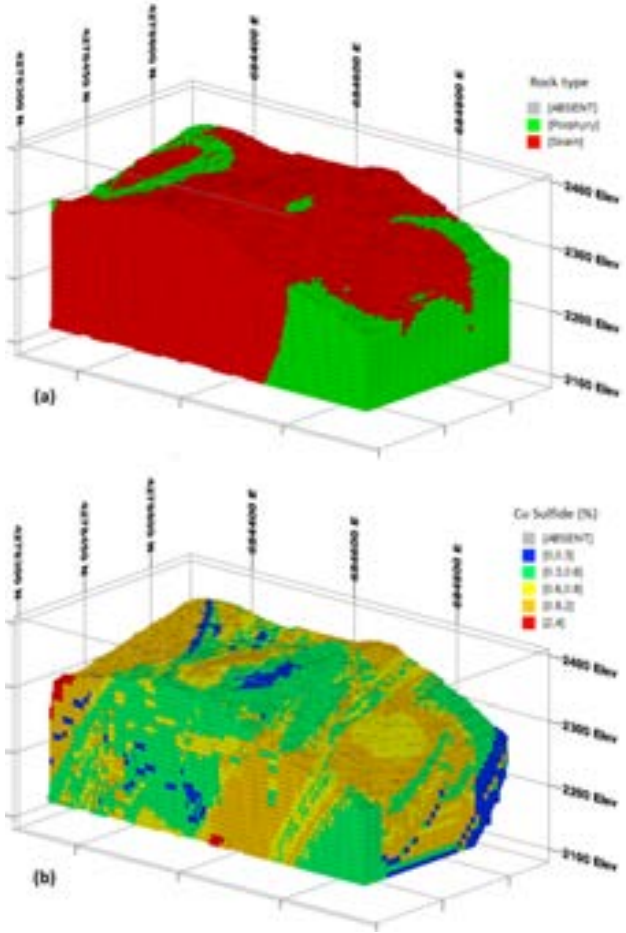

Figure 6. 3D visualization of the geological models of (a) rock types and (b) Cu grade.

Table 2. Parameters obtained for the variogram models of the Cu grade and rock type.

	Azimuth	Dip	Range (m)	sill	nugget	model
Cu Sulfide	60	60	90	0.3	0	spherical
Rock type	90	60	70	0.105	0.024	spherical

4.2. Geophysical models

According to the direction and nature of mineralization in the studied area, the geoelectrical survey was carried out with the aim of localizing sulfide copper mineralization. In order to acquire the data, a Scintrex IPR 12 equipment was used to conduct direct the current electrical tomography survey. There were seven electrical profiles to obtain information about the electrical resistivity (Rs) and induced polarization (IP) traits of sub-surface minerals (Figure 2b). The profiles were designed along an N-S direction. The pole-dipole array configuration was chosen for data acquisition according to the mineralization type, deposit situation, and surveying conditions. This array can achieve a greater depth of investigation, a more efficient field operation, and also a high rate of data collection. The approach developed by Loke [44] was run to invert the 2D electrical profiles.

In addition to electrical survey, the studied area was covered by a total magnetometry survey to determine the trend of mineralization. The magnetic survey was carried out using Scintrex-Envi Pro magnetometer. Station spacing was chosen about 3 m, while the average distance of profiles was about 50 m apart. Profiles were surveyed along an N-S direction (Figure 2b). The Earth's magnetic field has a declination and inclination angle of 57.7 and 5.8 degrees, respectively, with a background intensity of 49,045 nT. The approach proposed by Li and Oldenburg (1996) was utilized to generate the 3D model of the magnetic susceptibility property. The mesh size was designed in accordance with the studied area and the spacing of the data available in the region. The mesh height usually grows slightly with depth. When the surface topography of the area is present in the shallow region, the ratio of height to width of about 0.5 is suitable. However, at depth, a mesh height can be close to the mesh width [45]. The model domain for inverting the magnetic data was discretized into prismatic cells such that the core region spatially covered the entire survey area with 6-m cubic cells in the x (east), y (north), and z (depth) directions. Padding cells extending beyond the prospect region are designed to allow for any probable regional effect that might exist in the area. Cells above the topography were also removed from the model space. In addition to the magnetic susceptibility model, Salarian *et al*. (2019) has presented the procedure of inverting the electrical data in this region to generate the electrical models of resistivity and induced polarization [46].

The statistical features of Rs, IP, and magnetic susceptibility are given in Table 3. The histogram and box-plot of these geophysical variables are shown in Figure 4 (1^{st}, 2^{nd}, and 3^{rd} rows, respectively). After selecting the best directional variogram for implementing the kriging, the models of electrical properties were interpolated in 3D blocky models, similar to the one used in geological modeling. 3D inversion of the magnetic susceptibility model was also up-scaled to such blocky model through an OK method. This operation was carried out to unify all 3D models. The fitted variogram models for interpolating geophysical properties are shown in Figure 7. Table 4 lists the parameters of each variogram. The 3D estimations of geophysical properties are visualized in Figure 8.

Many models can reproduce data. However, some of them are not applicable for a particular application. Decreasing the number of acceptable models is necessary. It is an important requirement that the data obtained from the recovered model fits the survey data within an acceptable error range. The second important requirement is that the recovered model must be compatible with the geological conditions of the sub-surface. This requires the model to be smooth in all spatial directions. The predicted data should not match the observed data completely because if either is inaccurate, the recovered model will be wrong. The aim of the inversion is to reproduce the true data. True data means the data that would be measured if measurements are exact [47]. Figure 9 shows that the observed data and the predicted magnetometry data are in good agreement with each other. Electrical models could also predict appropriately original observations. (The interested readers are referred to the work by Salarian *et al*. 2019.) [46]. The cross-correlation plot between the observed and predicted magnetometry data is displayed in Figure 10. The Pearson's linear correlation coefficient between the observed magnetic data against the predicted data was obtained to be equal to +0.99.

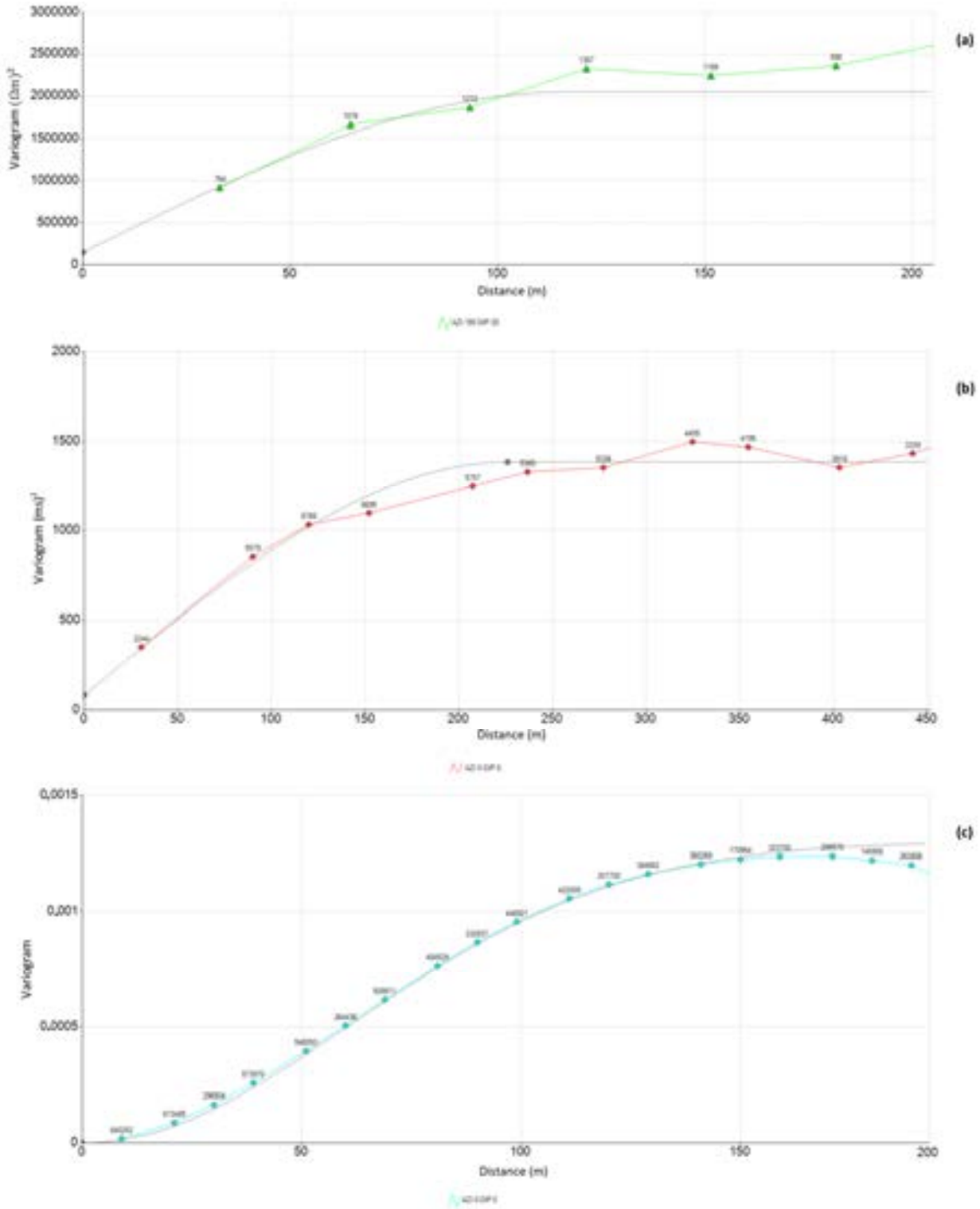

Figure 7. Experimental directional semi-variogram, models, and number of pairs for (a) electrical resistivity, (b) induced polarization, and (c) magnetic susceptibility.

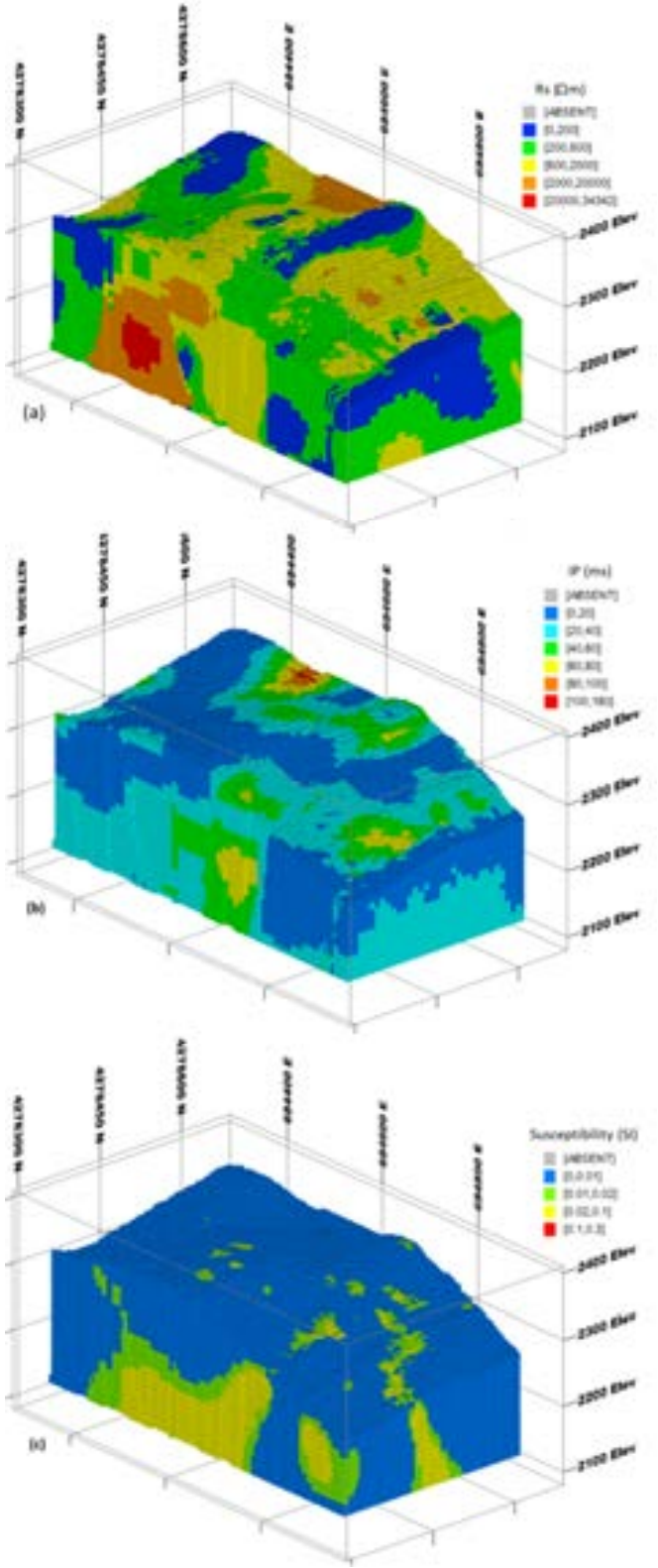

Figure 8. 3D visualization of geophysical models of (a) electrical resistivity, (b) chargeability, and (c) magnetic susceptibility.

Table 3. Statistical summary of geophysical variables.

	Number	Mean	Variance	Maximum	Upper quartile	Median	Lower quartile	Minimum
Rs (Ohm.m)	606	755.98	2.17E+06	16676.1	706.77	351.14	153.88	4.05
IP (ms)	606	37.52	1310.46	172.85	49.12	26.66	12.23	0.04
Susceptibility	330256	0.016	0.0011	0.228	0.015	0	0	0

Table 4. Parameters obtained for the variogram models of three geophysical variables.

	Azimuth	Dip	Range (m)	Sill	Nugget	Model
IP	0	0	225	1300	20	Spherical
Rs	180	20	117	2100000	148706	Spherical
Susceptibility	0	0	86	0.0013	0	Gaussian

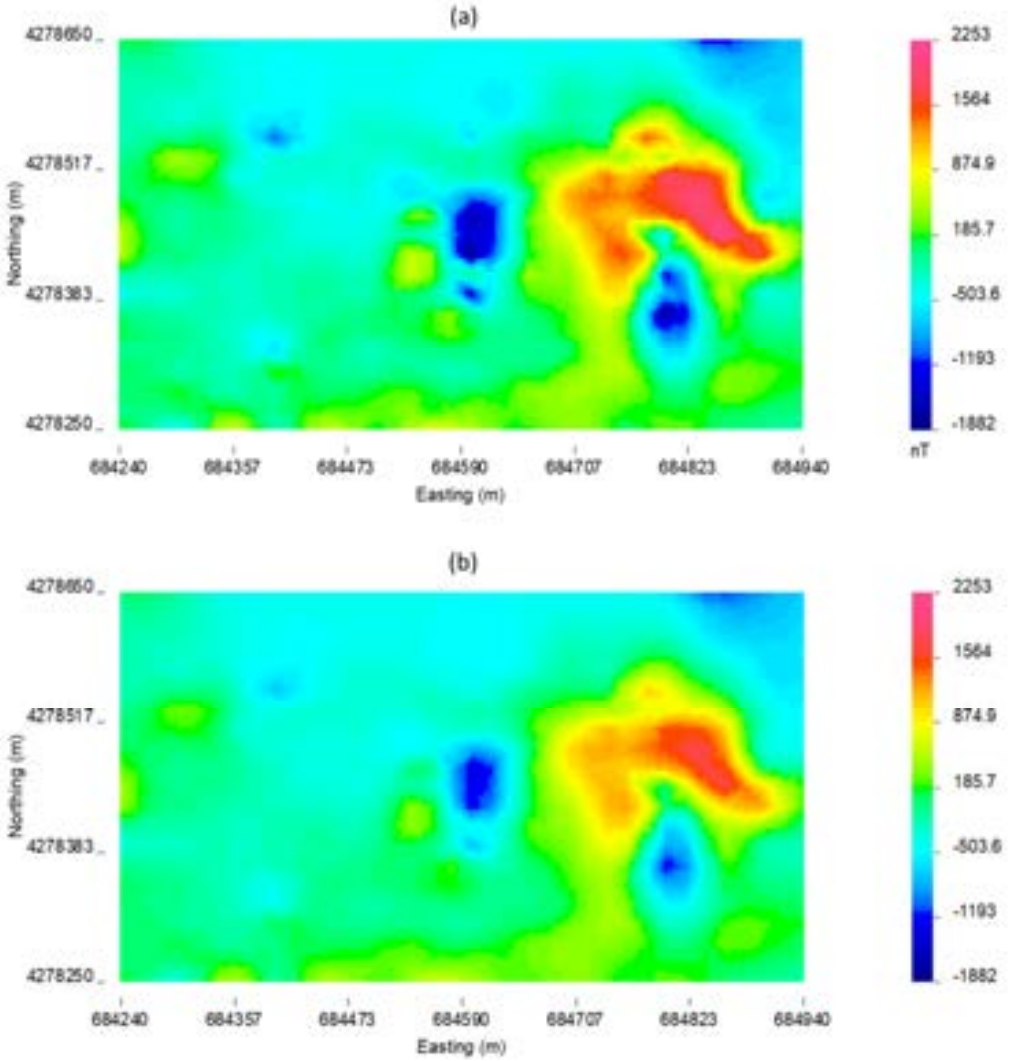

Figure 9. Maps of (a) the observed magnetic data and (b) the predicted data.

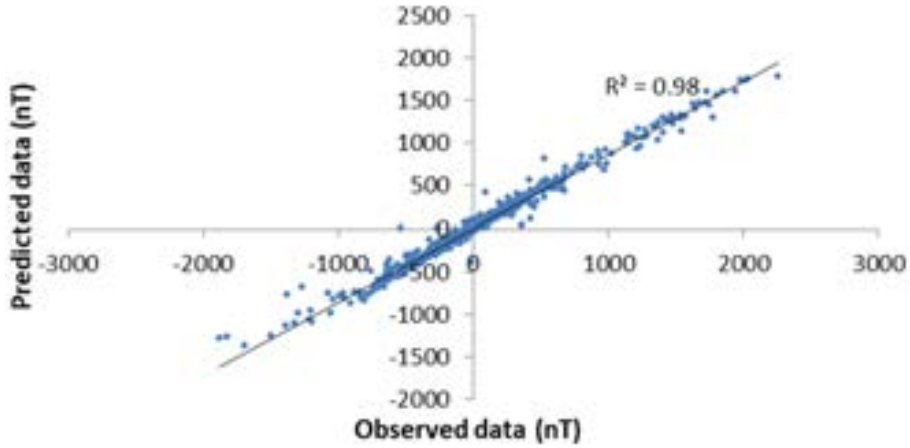

Figure 10. Scatter plot of the observed magnetic data against the predicted data.

5. Discussion

This section aims at investigating the spatial correlation of all constructed models of the electrical resistivity, chargeability, magnetic susceptibility, and Cu grade through a C-V multi-fractal analysis. As mentioned earlier, the block models were estimated via the OK and IK methods. Different volumes occupied by different values of concentration (values of models) were calculated for each geological and geophysical model. Hence, thresholds were recognized from log-log plots of the multi-fractal curve (Figure 11). These figures show a power-law relationship between the concentration of variables and the volume occupied. Break-points of the depicted lines in these figures show the threshold values. The break-points separate different line segments in the plots and divide each model into some subsets. Figure 11d shows that the Cu anomalous zone is defined by Cu grade greater than 1.85%. For these Cu concentrations, the slope of the straight line fit is close to the vertical angle. The first cut-off of the plot is 0.3%, which is interpreted as the threshold of barren host rocks or background for the ore element. The region between the first and second break-points from the left of the Cu log-log plot, i.e. Cu grade between 0.3% and 1%, can be interpreted as the porphyry zone. At the Cu grade equal to 1%, an enriched Cu mineralization (skarn zone) starts to build up. This is a new phase of mineralization separated from the porphyry regions. The threshold values from the C-V multi-fractal models of each variable are given in Table 5. It can be seen that the spatial variability of the element of interest behaves as multi-fractal nature. The skarn region begun from 1% Cu but an enriched part of skarn had a grade greater than 1.85%.

In order to investigate the subsets of each geophysical model and mineralized zones of Cu-bearing occurrence, the productivity variable was utilized. The productivity values were calculated by multiplying the Cu grade and length of the borehole samples (Table 6). The normalized productivity values for each geophysical fractal zone (ratio of productivity over the number of blocks per zone) have been superimposed on each subset/zone in Figure 11. Tables 7, 8, and 9 give the productivity scores in different zones of each geophysical model. The anomalous fractal zone for each model was highlighted according to the values for normalized productivity. The zone with the highest value for normalized productivity was chosen as the anomalous fractal zone.

The 3D visualizations of the multi-fractal zones of the geophysical models are shown in Figures 12-15, where each model was re-classified into new populations based on the fractal threshold values listed in Table 5. According to the productivity values, zones 1, 3, and 1 were selected as the anomalous zones for Rs, IP, and magnetic susceptibility, respectively. Figure 16 shows the anomalous zones for each 3D geophysical model. It seems that the final model of copper mineralization has a strike of E-W in close consistency with the models acquired from the geophysical properties. This meaningful correlation can localize the probable mineralization zones for further drilling to further envision of its mining potential.

The proportions of the skarn and porphyry rock types were calculated for each geophysical model in each fractal zone/subset. The results obtained are summarized in Table 10. The anomalous zones are shaded in gray in this table. Table 10 illustrates that the high ratios of the porphyry are in association with the low anomalous regions of resistivity, low anomalous regions of induced polarization, and high anomalous regions of magnetic susceptibility. The skarn mineralization show a reverse trend in comparison with the porphyry mineralization, where high proportions of the skarn are in association with the high values for electrical resistivity and induced polarization, and low values of magnetic susceptibility.

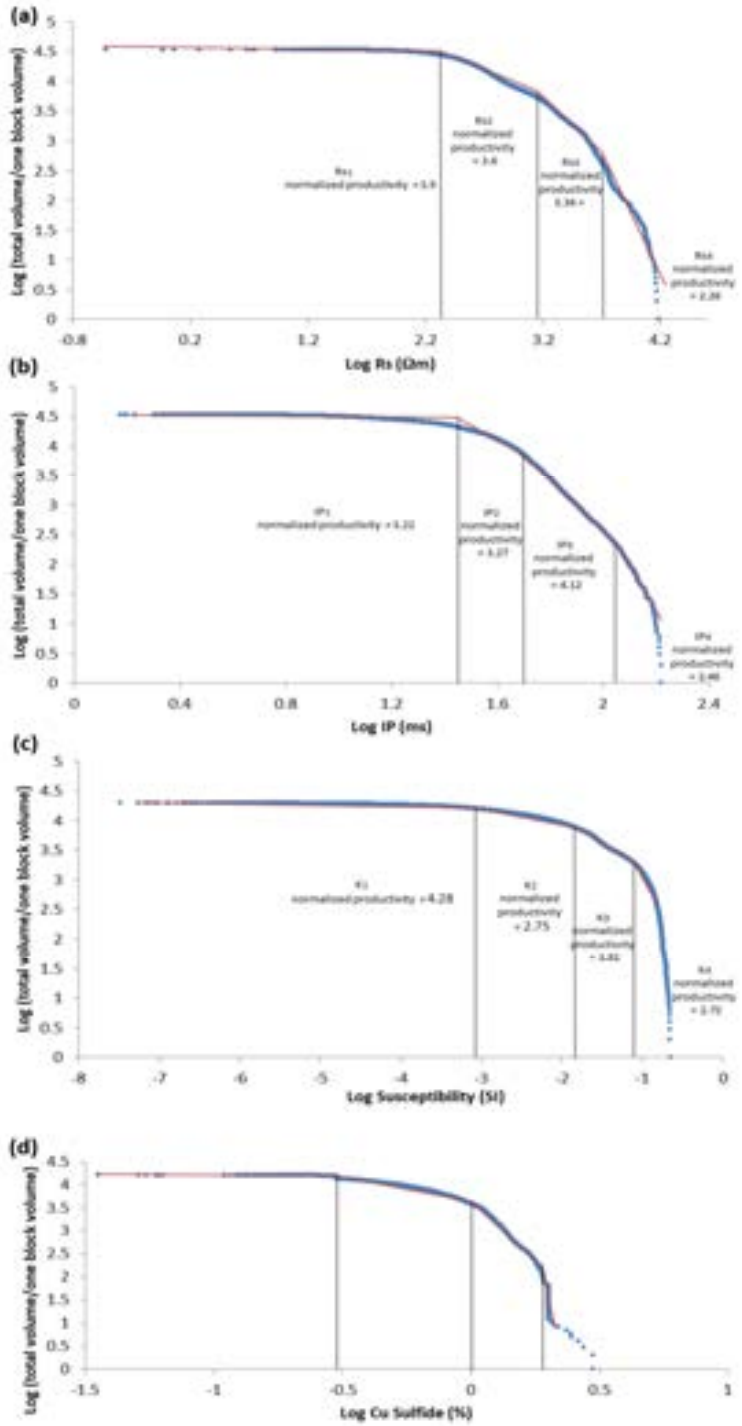

Figure 11. The C-V log-log plots of (a) electrical resistivity, (b) chargeability, (c) magnetic susceptibility, and (d) Cu grade. The normalized productivity values for each zone have been superimposed on the plots.

Table 5. Summary of threshold values from the C-V multi-fractal models for the electrical resistivity, chargeability, magnetic susceptibility, and Cu grade.

	Zone 1	Zone 2	Zone 3	Zone 4
Rs (ohm.m)	0	200	1584	4466
IP (ms)	0	28	50	112
Susceptibility	0	0.000794	0.0158	0.08
Cu Sulfide (%)	0	0.3	1	1.85

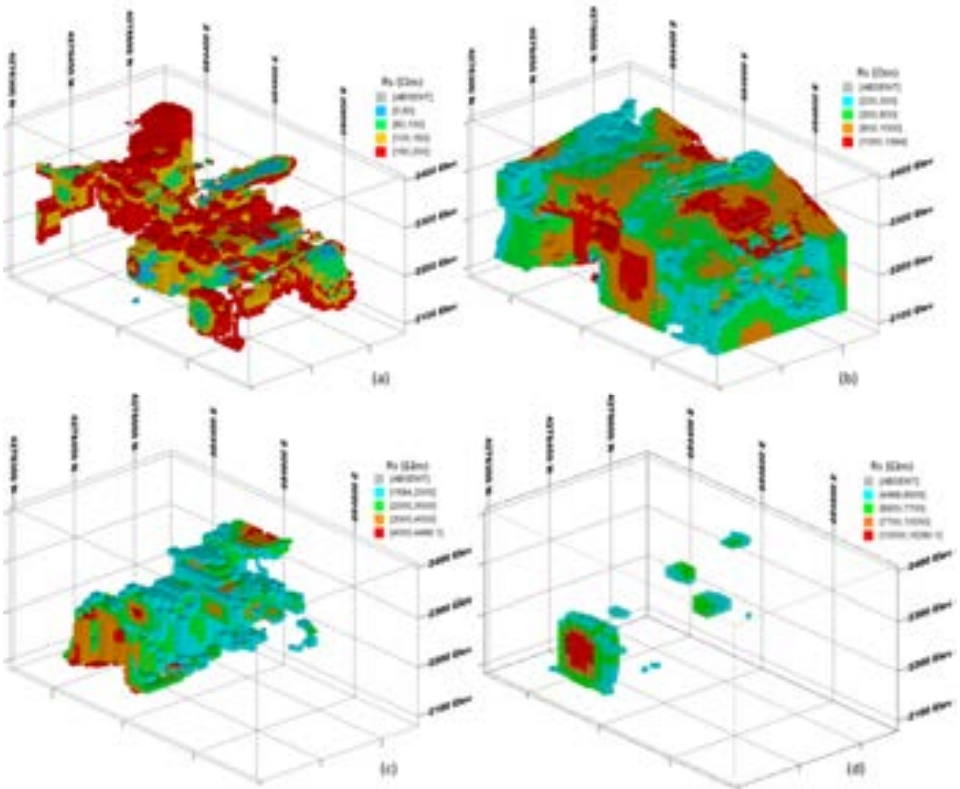

Figure 12. 3D visualization of the multi-fractal models of electrical resistivity, where each model has been re-classified into new populations based on the fractal threshold values (a) first fractal zone; (b) second fractal zone; (c) third fractal zone; and (d) fourth fractal zone.

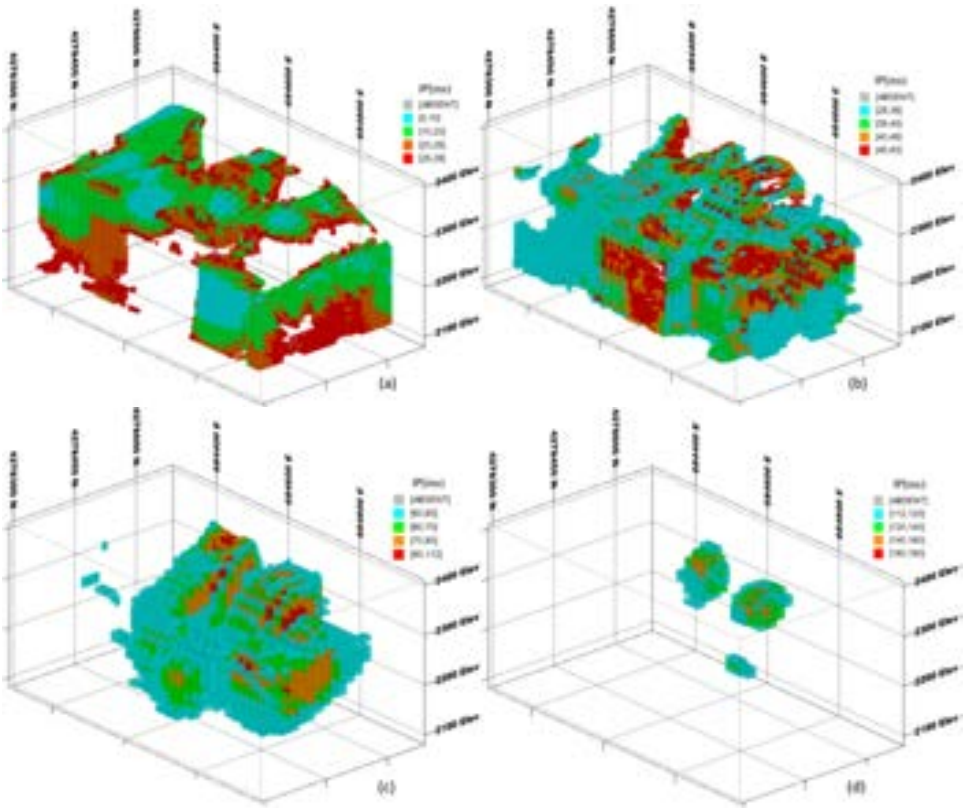

Figure 13. 3D visualization of the multi-fractal models of chargeability, where each model has been re-classified into new populations based on the fractal threshold values (a) first fractal zone; (b) second fractal zone; (c) third fractal zone; and (d) fourth fractal zone.

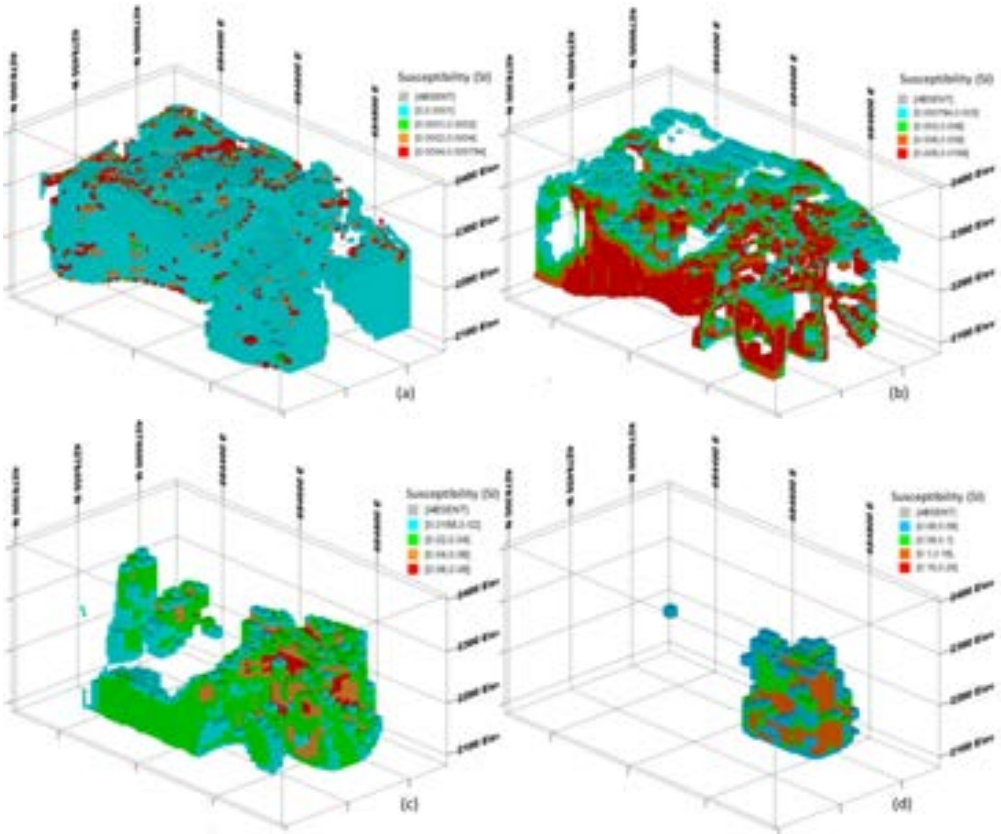

Figure 14. 3D visualization of the multi-fractal models of magnetic susceptibility, where each model has been re-classified into new populations based on the fractal threshold values (a) first fractal zone; (b) second fractal zone; (c) third fractal zone; and (d) fourth fractal zone.

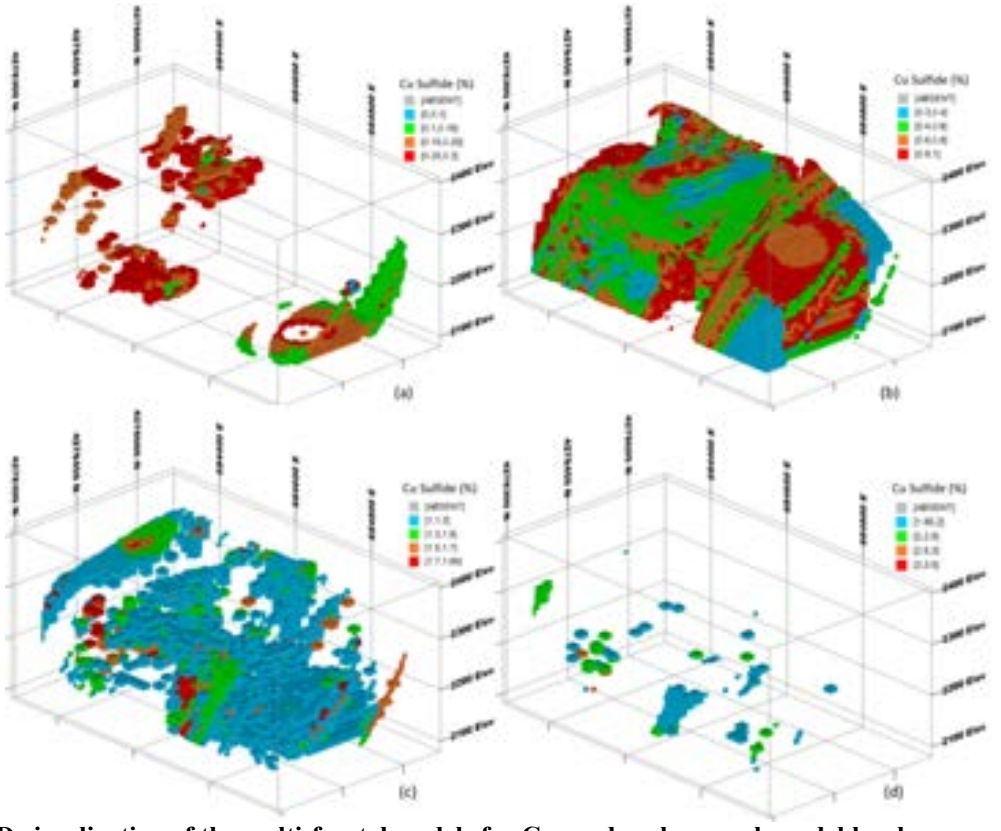

Figure 15. 3D visualization of the multi-fractal models for Cu grade, where each model has been re-classified into new populations based on the fractal threshold values (a) first fractal zone; (b) second fractal zone; (c) third fractal zone; and (d) fourth fractal zone.

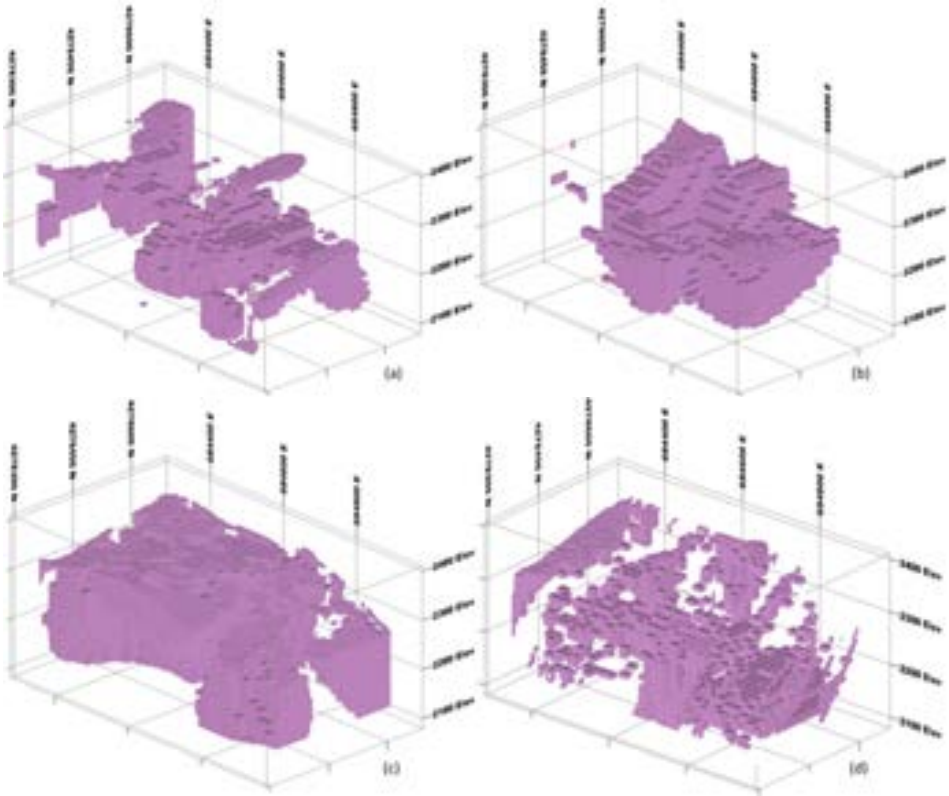

Figure 16. 3D visualization of anomalous zones for (a) electrical resistivity, (b) chargeability, (c) magnetic susceptibility, and (d) Cu grade.

Table 6. Results of drilled boreholes.

Borehole ID	X collar (m)	Y collar (m)	Z collar (m)	Borehole length (m)	Productivity (m.%)
BH 1	684630	4278350	2345	77.5	28.5
BH 2	684561	4278425	2364	68.6	64.3
BH 3	684600	4278444	2384	98	14
BH 4	684638	4278500	2387	82.5	0
BH 5	684583	4278455	2377	193	121.5835
BH 6	684577	4278373	2359	203	81.15
BH 7	684646	4278420	2362	187	145.45
BH 8	684690	4278455	2353	165.5	85.84
BH 9	684356	4278520	2340	190	67.32
BH 10	684475	4278440	2342	250	160
BH 11	684487	4278484	2341	220	118.44
BH 12	684473	4278379	2350	215	147.55
BH 13	684504	4278566	2261	250	167.53
BH 14	684541	4278342	2352	228.4	82.64
BH 15	684636	4278506	2367	135	59.66
BH 16	684846	4278481	2306	205	120.93

Table 7. Productivity scores in different zones of the electrical resistivity property.

	Zone 1	Zone 2	Zone 3	Zone 4
Productivity (m.%)	257.8	573.4	358	58.8
Number of blocks	66	159	107	26
Normalized Productivity (m.%)	3.9	3.6	3.34	2.26

Table 8. Productivity scores in different zones of the electrical chargeability property.

	Zone 1	Zone 2	Zone 3	Zone 4
Productivity (m.%)	512.68	327.5	511.3	44.28
Number of blocks	159	100	124	18
Normalized Productivity (m.%)	3.22	3.27	4.12	2.46

Table 9. Productivity scores in different zones of the magnetic susceptibility property.

	Zone 1	Zone 2	Zone 3	Zone 4
Productivity (m.%)	621	368	202	120
Number of blocks	145	134	53	44
Normalized Productivity (m.%)	4.28	2.74	3.81	2.72

Table 10. The proportion of each rock type for each zone of geophysical model. The most productive zone of each model has been highlighted by a shaded gray color.

	Zone 1	Zone 2	Zone 3	Zone 4
IP	47% Porphyry 53% Skarn	36% Porphyry 64% Skarn	7% Porphyry 93% Skarn	0% Porphyry 100% Skarn
Rs	40% Porphyry 60% Skarn	37% Porphyry 63% Skarn	13% Porphyry 87% Skarn	17% Porphyry 83% Skarn
Susceptibility	32% Porphyry 68% Skarn	34% Porphyry 66% Skarn	37% Porphyry 63% Skarn	50% Porphyry 50% Skarn

6. Conclusions

The performance of multi-fractal modeling of geological and geophysical characteristics was discussed in the East Azerbaijan Province in Iran for a porphyry-skarn Cu mineralization. Defining the exploration drilling targets couldn be better understood based on the geophysical fractal modeling. A geostatistical-based approach was utilized to generate the 3D geophysical and geological models. The 3D models of rock type, Cu grade, and three geophysical variables (electrical resistivity, chargeability, and magnetic susceptibility) were constructed using the kriging method. The C-V multi-fractal model revealed four different geophysical populations for each geophysical model. Choosing the geophysical anomalous zones from background zones was done based on the values of productivity criterion derived from exploratory drilling. The fractal zone with the highest score of productivity was selected as the anomalous zone.

The anomalous model of Cu mineralization had a distinct E-W strike in close consistency with the anomalous geophysical models. Such a meaningful correlation could localize the probable anomalous zones of mineralization for further exploratory drilling to seek its mining prospectivity of the desired region.

Finally, the relationship between the geophysical variables and the rock types was investigated for each fractal subset. The results obtained showed that the high proportions of the porphyry type were in association with the low anomalous regions of resistivity, low anomalous regions of induced polarization, and high anomalous regions of magnetic susceptibility. However, the skarn mineralization showed a completely reverse trend in comparison with the porphyry rock type.

Acknowledgments

The authors would like to express their sincere thanks to the School of Mining Engineering, University of Tehran, for all supports.

References

[1]. Caers, J. (2011). Modeling uncertainty in the earth sciences. John Wiley & Sons.

[2]. Lelièvre, P.G., Oldenburg, D.W. and Williams, N.C. (2009). Integrating geological and geophysical data through advanced constrained inversions. Exploration Geophysics. 40(4): 334-341.

[3]. Foged, N., Marker, P.A., Christiansen, A.V., Bauer-Gottwein, P., Jørgensen, F., Høyer, A.S. and Auken, E. (2014). Large-scale 3-D modeling by integration of resistivity models and borehole data through inversion. Hydrology and Earth System Science. 18 (11): 4349-4362.

[4]. Reynolds, J.M. (2011). An introduction to applied and environmental geophysics. John Wiley & Sons.

[5]. Loke, M., Chambers, J., Rucker, D., Kuras, O. and Wilkinson, P. (2013). Recent developments in the direct-current geoelectrical imaging method. Journal of applied geophysics. 95: 135-156.

[6]. Mashhadi, S. and Ramazi, H. (2018). The Application of Resistivity and Induced Polarization Methods in Identification of Skarn Alteration Haloes: A Case Study in the Qale-Alimoradkhan Area. Journal of Environmental Engineering Geophysics. 23 (3): 363-368.

[7]. Telford, W.M., Geldart, L.P. and Sheriff, R.E. (1990). Applied geophysics. 2nd edition edn. Cambridge University Press.

[8]. Pelton, W.H., Ward, S., Hallof, P., Sill, W. and Nelson, P.H. (1978). Mineral discrimination and removal of inductive coupling with multifrequency IP. Geophysics. 43 (3): 588-609.

[9]. Vanhala, H. and Peltoniemi, M. (1992). Spectral IP studies of Finnish ore prospects. Geophysics. 57 (12): 1545-1555.

[10]. Emerson, D. (1986). Physical properties of skarns. Exploration Geophysics. 17 (4): 201-212.

[11]. Sawkins, F.J. (2013). Metal deposits in relation to plate tectonics. Springer Science & Business Media.

[12]. Gunn, P. and Dentith, M. (1997). Magnetic responses associated with mineral deposits. AGSO Journal of Australian Geology. 17: 145-158.

[13]. Goncalves, M.A., Mateus, A. and Oliveira, V. (2001). Geochemical anomaly separation by multifractal modelling. Journal of Geochemical Exploration. 72 (2): 91-114.

[14]. Ni, C., Zhang, S., Chen, Z., Yan, Y. and Li, Y. (2017). Mapping the Spatial Distribution and Characteristics of Lineaments Using Fractal and Multifractal Models: A Case Study from Northeastern Yunnan Province, China. Scientific reports. 7 (1): 10511.

[15]. Scholz, C. and Mandelbrot, B. (1992). Special issue on fractals in geology and geophysics. Pure Appl Geophys. 131: 96-171.

[16]. Turcotte, D.L. (1997). Fractals and chaos in geology and geophysics. Cambridge university press.

[17]. Dimri,V. (2005). Fractal behaviour of the earth system. Springer.

[18]. Malamud, B.D. and Turcotte, D.L. (1999). Self-affine time series: I. Generation and analyses. In: Advances in Geophysics. Vol 40. Elsevier. pp 1-90.

[19]. Daneshvar Saein, L., Rasa, I., Rashidnejad Omran, N., Moarefvand, P. and Afzal, P. (2012). Application of concentration-volume fractal method in induced polarization and resistivity data interpretation for Cu-Mo porphyry deposits exploration, case study: Nowchun Cu-Mo deposit, SE Iran. Nonlinear Processes in Geophysics. 19 (4): 431-438.

[20]. Turcotte, D.L. (2004). The relationship of fractals in geophysics to “the new science”. Chaos, Solitons Fractals. 19 (2): 255-258.

[21]. Afzal, P., Alghalandis, Y.F., Khakzad, A., Moarefvand, P. and Omran, N.R. (2011). Delineation of mineralization zones in porphyry Cu deposits by fractal concentration–volume modeling. Journal of Geochemical Exploration. 108 (3): 220-232.

[22]. Delavar, S.T., Afzal, P., Borg, G., Rasa, I., Lotfi, M. and Omran, N.R. (2012). Delineation of mineralization zones using concentration–volume fractal method in Pb–Zn carbonate hosted deposits. Journal of Geochemical Exploration. 118: 98-110.

[23]. Yasrebi, A.B., Afzal, P., Wetherelt, A., Foster, P. and Esfahanipour, R. (2013). Correlation between geology and concentration-volume fractal models: significance for Cu and Mo mineralized zones separation in the Kahang porphyry deposit (Central Iran). Geologica Carpathica. 64 (2): 153-163.

[24]. Abedi, M., Asghari, O. and Norouzi, G.H. (2015). Collocated cokriging of iron deposit based on a model of magnetic susceptibility: a case study in Morvarid mine, Iran. Arabian Journal of Geosciences. 8 (4): 2179-2189.

[25]. Asghari, O., Sheikhmohammadi, S., Abedi, M. and Norouzi, G. (2016). Multivariate geostatistics based on a model of geo-electrical properties for copper grade estimation: a case study in Seridune, Iran. Bollettino di Geofisica Teorica ed Applicata. 57 (1).

[26]. Webster, R. and Oliver, M.A. (2001). Geostatistics for environmental scientists (Statistics in Practice).

[27]. Rossi, M.E. and Deutsch, C.V. (2013). Mineral resource estimation. Springer Science & Business Media.

[28]. Journel, A.G. (1983). Nonparametric estimation of spatial distributions. Journal of the International Association for Mathematical Geology. 15 (3): 445-468.

[29]. Glacken, I. and Blackney, P. (1998). A practitioners implementation of indicator kriging. In: Proceedings of a one day symposium: Beyond Ordinary Kriging.

[30]. Goovaerts, P. (1997). Geostatistics for natural resources evaluation. Oxford University Press on Demand.

[31]. Cheng, Q., Agterberg, F. and Ballantyne, S. (1994). The separation of geochemical anomalies from background by fractal methods. Journal of Geochemical Exploration. 51 (2): 109-130.

[32]. Zuo, R., Cheng, Q. and Xia, Q. (2009). Application of fractal models to characterization of vertical distribution of geochemical element concentration. Journal of Geochemical Exploration. 102 (1): 37-43.

[33]. Stöcklin, J. (1968). Structural history and tectonics of Iran. 52 (7): 1229-1258.

[34]. Berberian, F. and Berberian, M. (1981). Tectono-plutonic episodes in Iran. Zagros Hindu Kush Himalaya Geodynamic Evolution. 3: 5-32.

[35]. Nouri, F., Azizi, H., Stern, R.J., Asahara, Y., Khodaparast, S., Madanipour, S. and Yamamoto, K. (2018). Zircon U-Pb dating, geochemistry and evolution of the Late Eocene Saveh magmatic complex, central Iran: Partial melts of sub-continental lithospheric mantle and magmatic differentiation. Lithos. 314: 274-292.

[36]. Berberian, M. and King, G. (1981). Towards a paleogeography and tectonic evolution of Iran. Canadian journal of earth sciences. 18 (2): 210-265.

[37]. Rezaei, S., Lotfi, M., Afzal, P., Jafari, M.R., Meigoony, M.S. and Khalajmasoumi, M. (2015). Investigation of copper and gold prospects using index overlay integration method and multifractal modeling in Saveh 1: 100,000 sheet, Central Iran. Gospodarka Surowcami Mineralnymi. 31 (4): 51-74.

[38]. Shahabpour, J. (2005). Tectonic evolution of the orogenic belt in the region located between Kerman and Neyriz. Journal of Asian Earth Sciences. 24 (4): 405-417.

[39]. Kazemi, K., Kananian, A., Xiao, Y. and Sarjoughian, F. (2018). Petrogenesis of Middle-Eocene granitoids and their Mafic microgranular enclaves in central Urmia-Dokhtar Magmatic Arc (Iran): evidence for interaction between felsic and mafic magmas. Geoscience Frontiers. 10 (2): 705-723.

[40]. Richards, J.P., Wilkinson, D. and Ullrich, T. (2006). Geology of the Sari Gunay epithermal gold deposit, northwest Iran. Economic Geology. 101 (8): 1455-1496.

[41]. Mehrabi, E., Masoudi, F., Jamali, H. and Asgharzadeh, H. (2013). Petrography, alteration, and mineralization of Agh-Daragh region. In: 17th Conference of Iranian Geological Society, Tehran, Iran.

[42]. Kazem Alilou, S., Abedi, M., Norouzi, G. and Dowlati, F. (2012). Application of magnetometery, special resistivity and induced polarization for exploration of iron and copper skarn deposits, a case study: Ghalandar, Ahar. In: 1th national conference of exploration engineering, University of Shahroud, Iran.

[43]. Alilou, S.K. (2015). Application of Fuzzy decision making approach in 2D mineral potential mapping and its comparison with 3D magnetic geophysical presentation in Ghalandar Zone, West Azerbaijan province of Iran. In. Vol MSc. University of Tehran, Tehran, Iran.

[44]. Loke, M. (2004). Tutorial: 2-D and 3-D electrical imaging surveys.

[45]. Li, Y. and Oldenburg, D.W. (1996). 3-D inversion of magnetic data. Geophysics. 61 (2): 394-408.

[46]. Salarian, S., Asghari, O., Abedi, M. and Alilou, S.K. (2019). Geostatistical-based geophysical model of electrical resistivity and chargeability to image Cu mineralization in Ghalandar deposit, Iran. International Journal of Mining and Geo-Engineering (in press).

[47]. Lelièvre, P.G. (2003). Forward modelling and inversion of geophysical magnetic data. In. University of British Columbia.

مدل‌سازی مولتی فرکتال و زمین‌آماری ویژگی‌های ژئوفیزیکی و زمین‌شناسی کانسار مس اسکارن- پورفیری منطقه قلندر، ایران

سیاوش سالاریان[۱]، امید اصغری[۱*]، میثم عابدی[۲] و سعید کاظم علیلو[۳]

۱- آزمایشگاه شبیه‌سازی و پردازش داده، دانشکده مهندسی معدن، دانشگاه تهران، ایران
۲- آزمایشگاه اکتشافات هدفمند، دانشکده مهندسی معدن، دانشگاه تهران، ایران
۳- دانشکده مهندسی معدن، دانشگاه تهران، ایران

ارسال ۲۰۱۹/۷/۱۲، پذیرش ۲۰۱۹/۸/۸

* نویسنده مسئول مکاتبات: o.asghari@ut.ac.ir

چکیده:

هدف از این پژوهش، به تصویر کشیدن ارتباط فضایی بین مدل‌های زمین‌شناسی و ژئوفیزیکی کانی‌زایی مس سولفیدی از طریق آنالیز سه‌بعدی تلفیقی هدف مورد نظر است. کانسار اسکارن- پورفیری مس قلندر که در شمال غربی ایران واقع شده است، برای این کار انتخاب شده است. سه برداشت ژئوفیزیکی مقاومت الکتریکی جریان مستقیم و توموگرافی قطبش القایی همراه با مغناطیس‌سنجی به ترتیب برای ساختن ویژگی‌های فیزیکی مقاومت الکتریکی، شارژابیلیتی و خودپذیری مغناطیسی انجام شده است. مدل‌سازی معکوس و درون‌یابی زمین‌آماری برای ساخت مدل‌های سه‌بعدی فیزیکی به کار گرفته شد. مدل سه‌بعدی عیار مس به روش کریگینگ معمولی ساخته شده است. همچنین برای طراحی مدل سه‌بعدی نوع سنگ با استفاده از داده‌های حفاری، از روش کریگینگ شاخص استفاده شده است. به منظور بررسی ارتباط بین ویژگی‌های ژئوفیزیکی و زمین‌شناسی در کانی‌زایی مس، مدل‌های بلوکی خصوصیات ژئوفیزیکی و زمین‌شناسی در یک مدل بلوکی با اندازه سلول‌های مشابه قرار داده شده است. روش مولتی‌فرکتال عیار- حجم برای تبدیل هر مدل به زیرمجموعه‌های کوچک‌تر استفاده شده است و منطقه فرکتالی که بیشترین میزان بهره‌وری برای تولید مس را دارا است، شناسایی شده است. نتایج نشان داد که زیرمجموعه‌های مدل‌های ژئوفیزیکی به طور فضایی با مدل‌های زمین‌شناسی عیار مس و نوع سنگ در ارتباط هستند. مناطقی که مقاومت الکتریکی کم، شارژابیلیتی زیاد و خودپذیری مغناطیسی کم دارند، با منبع اصلی کانی‌زایی مس (غالباً اسکارن) مطابق هستند.

کلمات کلیدی: مدل مولتی‌فرکتال، زمین‌آمار، شارژابیلیتی الکتریکی، مقاومت الکتریکی، خودپذیری مغناطیسی.